Journal of Biomedical and Translational Research
pISSN 2508-1357 eISSN 2508-139X

Original Article
J Biomed Transl Res 2025;26(4):159-171
https://doi.org/10.12729/jbtr.2025.26.4.159

# Development of translational murine soft tissue defect model for wound healing research

Yo Han Min[1,2], Jinyeong Lim[2], Sol Lee[2], Seong Soo Kang[1,2*], Kyung Mi Shim[1,2*]

[1]*Department of Veterinary Surgery, College of Veterinary Medicine and BK21 Plus Project Team, Chonnam National University, Gwangju 61186, Korea*
[2]*Biomaterial R&BD Center, Chonnam National University, Gwangju 61186, Korea*

Received: Dec 2, 2025
Revised: Dec 8, 2025
Accepted: Dec 8, 2025

***Corresponding author**
Seong Soo Kang
Department of Veterinary Surgery, College of Veterinary Medicine and BK21 Plus Project Team, Chonnam National University, Gwangju 61186, Korea
Tel: +82-62-530-2877
E-mail: vetkang@chonnam.ac.kr

Kyung Mi Shim
Department of Veterinary Surgery, College of Veterinary Medicine and BK21 Plus Project Team, Chonnam National University, Gwangju 61186, Korea
Tel: +82-62-530-2889
E-mail: simchung-98@hanmail.net



**ORCID**
Yo Han Min
https://orcid.org/0009-0007-2913-9056
Jinyeong Lim
https://orcid.org/0000-0002-7006-1875
Sol Lee
https://orcid.org/0000-0003-0452-9625
Seong Soo Kang
https://orcid.org/0000-0002-8957-0354
Kyung Mi Shim
https://orcid.org/0000-0002-2273-6655

**Conflict of Interest**
No potential conflict of interest relevant to this article was reported.

## Abstract

Extensive soft tissue defects involving loss of skin, fat, and muscle often result from trauma or tumor resection. Current treatments, including autografts and flaps, are limited by donor-site morbidity and scarce tissue availability. Animal models, particularly in rodents, are essential for research but are limited by their primary healing mechanism—contraction via the panniculus carnosus—which does not accurately reflect human healing. Furthermore, standardized models for complex skin–muscle defects are lacking. Therefore, this study aims to create a clinically relevant composite soft tissue defect model in mice using a three-dimensional (3D) polylactic acid (PLA) chimney splint to inhibit contraction and better mimic human wound healing mechanisms (re-epithelialization and granulation tissue formation). A composite defect was created on the dorsum of 8-week-old BALB/c nude mice. The biocompatibility of the 3D-printed PLA chimney was assessed via MTT assay. *In vivo*, fixation methods—tissue adhesive (TA), simple interrupted sutures (SI), and purse-string suture (PS)—were compared. Wound healing was evaluated over 4 weeks via gross and histological analyses. PLA material showed excellent biocompatibility *in vitro*, with cell viability consistently above 85%, indicating noncytotoxicity. *In vivo*, the TA and SI groups showed severe inflammation, tissue necrosis, and splint detachment. In contrast, the PS group remained stable for 4 weeks with no complications. Histologically, the PS group effectively suppressed contraction. Re-epithelialization from the wound edge, well-organized granulation tissue with active angiogenesis, abundant fibroblasts, and collagen deposition, and spindle-shaped cells were clearly observed. In conclusion, this study establishes a reproducible and stable murine composite soft tissue defect model by combining a 3D-printed chimney splint with a PS technique. This model overcomes a key limitation of rodent wound models by controlling contraction, offering a robust preclinical platform to study composite tissue healing and evaluate next-generation regenerative medicine therapies.

**Keywords:** wounds and injuries; translational science, biomedical; three-dimensional; splints; mice

## INTRODUCTION

Extensive soft tissue defects entail the loss of multiple tissues—skin, subcutaneous fat, muscle, and blood vessels—often caused by trauma, burns, tumor resection, or chronic disease. Minor

**Acknowledgements**
Not applicable.

**Ethics Approval**
The animal study was approved by the Institutional Animal Care and Use Committee of Chonnam National University in Korea (Approval No. CNU IACUC-YB-2024-42).

tissue damage may heal naturally, but extensive injuries such as critical-size defects often result in incomplete healing, severe scarring, or chronic infection, impairing significant function and appearance. Currently, the clinical gold standard for treating these defects is autografts and surgical flaps. However, these methods are limited by donor site morbidity, limited tissue availability, and surgical complexity. Research is currently ongoing to clarify wound healing mechanisms and develop effective treatment strategies [1–3].

Animal models are essential for these research processes. Studies have focused on developing animal models of skin or muscle defects. In models with defects limited to skin or muscle, research has primarily evaluated healing using tissue-engineered scaffolds, induced pluripotent stem cells, and extracellular matrix components [3–8]. However, most soft tissue injuries encountered in clinical practice are complex, affecting skin and muscle layers rather than a single tissue type. Despite its clinical relevance, an experimentally standardized and reproducible animal model that simultaneously includes skin and muscle defects has not yet been fully established.

Rodents are the most commonly used animal models for wound healing research because they are affordable, easily genetically manipulated, and have a short lifespan. However, their skin has a unique structure that differs from human skin, notably due to the presence of a muscle layer called the panniculus carnosus. This layer enables their skin to slide over the subcutaneous fascia and contract, promoting rapid wound closure through epithelial contraction. In contrast, human wound healing relies mainly on re-epithelialization and granulation tissue formation, making direct translation of rodent findings to humans challenging [9–12].

To address these limitations and better mimic human wound healing, various methods have been developed to inhibit mechanical wound contraction. A prominent example is the splint model, in which a silicone ring or frame is secured around the wound. This model suppresses panniculus carnosus muscle activity, promoting healing through re-epithelialization and granulation tissue formation [13–15]. However, conventional splint models primarily target the skin layer and fail to adequately replicate composite injuries that involve deeper muscle tissue.

Furthermore, replicating defects in the skin and underlying muscle layers is clinically important. Volumetric muscle loss (VML), resulting from trauma or tumor resection, rarely regenerates spontaneously and frequently leads to severe functional impairment [7]. Existing VML models have largely focused on muscle regeneration, while the development of composite soft tissue defect models that simultaneously involve skin and muscle remains limited. Thus, an animal model that integrates anti-contraction control and deep tissue injury is urgently needed to allow a more physiologically relevant assessment of composite tissue healing.

Therefore, this study aims to develop a reproducible, clinically relevant mouse model of extensive soft tissue defects encompassing skin and muscle layers. A 3D-printed chimney was used to regulate wound contraction. Compared to traditional silicone-based splints, this 3D-printed approach allows precise control of defect geometry, improved reproducibility, and greater stability during long-term observation. By incorporating muscle loss beneath the skin defect, we seek to create an integrated composite wound model that closely mimics clinically observed injuries. This model could serve as a valuable platform for elucidating skin–muscle


https://doi.org/10.12729/jbtr.2025.26.4.159

interactions during healing and for evaluating the preclinical efficacy of emerging regenerative medicine and tissue engineering strategies.

## MATERIALS AND METHODS

### Fabrication of the 3D-printed chimney/lid

A chimney-shaped 3D-printed splint was used to establish a mouse wound model by preventing contraction through healing, the primary healing mechanism in rodents. The chimney was 3D-printed from medical-grade polylactic acid (PLA) using a Raise3D Pro2 printer (Raise3D Technologies, Lake Forest, CA, USA; Fig. 1). The process included size adjustments to ensure a proper fit for the mouse wound and was conducted in three stages (Fig. 2). After selecting the appropriate chimney size, the design was modified to match the chosen fixation method for securing it to the mouse. The fabricated chimney and lid were cleaned using an ultrasonic cleaner (POWERSONIC 410, Hwashin Tech, Seoul, Korea) and sterilized using an ethylene oxide gas sterilizer (HS-3241EO, Hanshin Medical, Incheon, Korea).

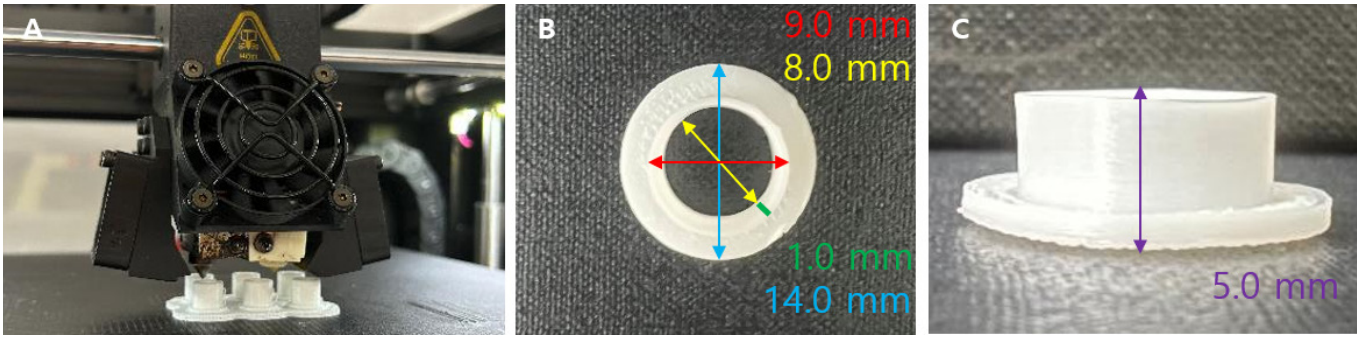


**Fig. 1. Procedure of chimney manufacture.** (A) Photograph of the chimney manufactured using a 3D-printer. (B) Top-view measurement of the chimney dimensions. (C) Side-view measurement of the chimney dimensions. 3D, three-dimensional.

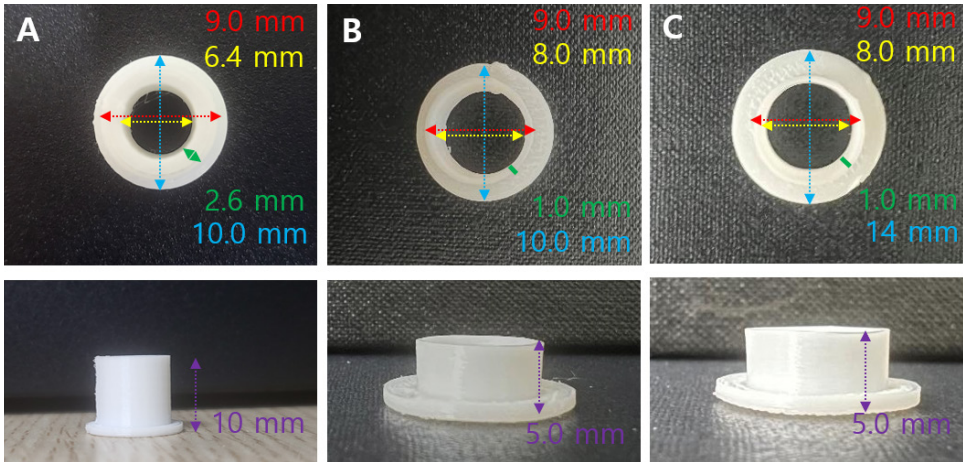


**Fig. 2. Photographs showing the evolution of PLA chimney sizes.** (A) First manufactured chimney: outer diameter 9 mm, inner diameter 6.4 mm, wing diameter 10 mm, chimney thickness 2.6 mm, chimney height 10 mm. (B) Second manufactured chimney: outer diameter 9 mm, inner diameter 8 mm, wing diameter 10 mm, chimney thickness 1 mm, chimney height 5 mm. (C) Third manufactured chimney: outer diameter 9 mm, inner diameter 8 mm, wing diameter 14 mm, chimney thickness 1 mm, chimney height 5 mm. PLA, polylactic acid.

To develop the most suitable fixation design, various chimney shapes were fabricated. The designs featured wings with 0, 2, or 4 suture holes to accommodate different fixation strategies (Fig. 3). A mesh-topped lid was later added to the hole-free chimney design to improve ventilation and enable wound inspection, and additional experiments were performed. The final optimized chimney measured 9 mm in outer diameter, 8 mm in inner diameter, 14 mm in wing diameter, and 5 mm in height. A matching mesh-topped lid measuring 10 mm in outer diameter, 9 mm in inner diameter, and 3.5 mm in height was also fabricated and used in the experiments.

## *In vitro* polylactic acid evaluation

### *Cytotoxicity test*

Cytotoxicity was assessed in L-929 mouse fibroblasts using the MTT assay according to ISO 10993-5 (KCLB, Seoul, Korea). Four experimental groups were prepared: control, negative control, positive control, and PLA chimney. Extracts were prepared in minimum essential medium (Gibco, Thermo Fisher Scientific, Waltham, MA, USA) and applied to cells in 96-well plates. After 24 hr incubation, optical density (OD) at 570 nm was measured using a microplate reader (SpectraMax i3x, Molecular Devices, San Jose, CA, USA). Cell viability (%) was calculated using the following formula:

$$\text{Cell viability (\%)} = 100 \times \frac{\text{OD570e}}{\text{OD570b}} \qquad (1)$$

Values below 70% were considered cytotoxic, and statistical analysis was performed using one-way ANOVA ($^{**}p<0.01$, $^{***}p<0.001$).

## *In vivo* study in mice

### *Experimental animals*

Twelve male BALB/c nude mice (≈21 ± 3 g, 8 weeks old; Orient Bio, Seongnam, Korea) were used in the experiment. All experiments were approved by the Institutional Animal Care and Use Committee of Chonnam National University (CNU IACUC-YB-2024-42). Mice had *ad libitum* access to laboratory chow and water and were housed under controlled conditions at

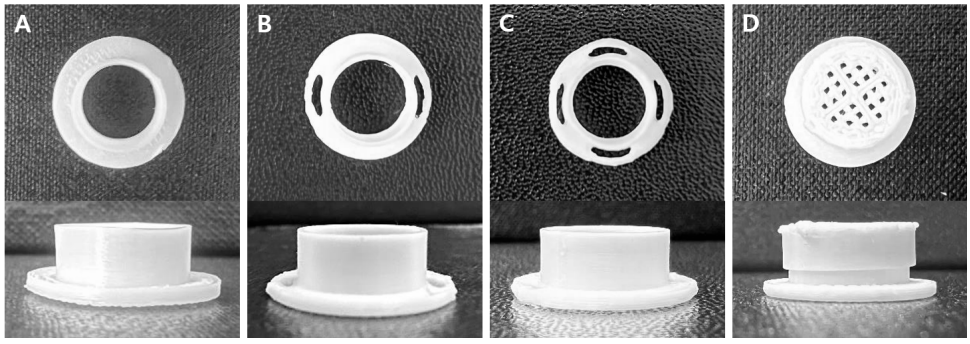


**Fig. 3. Photographs illustrating the design evolution of the PLA chimney.** (A) Top and side views of the chimney without holes. (B) Top and side views of the chimney with two holes. (C) Top and side views of the chimney with four holes. (D) Top and side views of the chimney (no hole) with lid. PLA, polylactic acid.


https://doi.org/10.12729/jbtr.2025.26.4.159

20 ± 3°C and 50 ± 10% humidity. Test groups were established as follows: tissue adhesive (TA), TA + simple interrupted (SI; 2 sites), TA + SI (4 sites), and purse-string suture (PS; Table 1).

### *Extensive soft tissue defect formation and chimney application*

After 1 week of acclimation, the mice underwent procedures to create extensive wounds. Before anesthesia, mice were placed in an anesthesia induction chamber and sedated with 2%–3% sevoflurane (Sevofran Liq., Hana Pharm, Hwaseong, Korea). They were premedicated with tramadol HCl 25 mg/kg intraperitoneally (IP; Maritrol Inj, Jeil Pharmaceutical, Seoul, Korea) and enrofloxacin 5 mg/kg subcutaneously (SC; Baytril® 50 Inj, Elanco Korea, Seoul, Korea) for easier handling. Anesthesia was induced via IP administration of xylazine 10 mg/kg (Rompun® 100 mg/mL, Elanco Korea, Seoul, Korea) and ketamine 100 mg/kg (Yuhan Ketamine 50 Inj., Yuhan Corporation, Seoul, Korea). If necessary, atropine 0.4 mg/kg (Atropine sulfate Inj, Jeil Pharmaceutical, Seoul, Korea) was administered SC to maintain blood pressure and heart rate during anesthesia. After drug administration, Liposic ophthalmic gel (10 g; Bausch Health Korea, Seoul, Korea) was applied to the eyes, and the dorsal skin was disinfected with 10% povidone-iodine and 70% alcohol.

A 10 mm skin defect (full-thickness) was surgically created on the dorsal surface, along with an 8 mm defect in the underlying muscle, including the gluteus and quadriceps femoris muscles. For extensive bleeding unresponsive to compression epinephrine (Bosmin Sol; Jeil Pharmaceutical, Seoul, Korea) was applied for additional hemostasis (Fig. 4). The 3D-printed chimney was secured to the skin wound using 4-0 polyamide sutures (SI or PS sutures; Dafilon® 4/0, B. Braun Surgical, Barcelona, Spain) or a TA (Dopasolution, Science Begins, Seoul, Korea). The chimney top was then covered with a 3D-printed lid or dressing material (3M™ Tegaderm™, Minnesota Mining and Manufacturing Company, Saint Paul, MN, USA) to prevent wound desiccation and infection (Fig. 5).

### *Postoperative care and follow-up evaluations*

For hydration, normal Saline (6 mL/kg; Normal saline Inj., [100 mL], JW Pharmaceutical Corporation, Gwacheon, Korea) was administered SC. When recover from anesthesia was required, atipamezole (1 mg/kg; Antisedan®, Zoetis KR, Seoul, Korea) was diluted and injected intramuscularly. Tramadol (5 mg/kg; Tridol SR tab [100 mg], Yuhan, Seoul, Korea) and enrofloxacin (5 mg/kg; Baytril® flavor tab, 50 mg, Elanco Korea, Seoul, Korea) were combined in drinking water at a 5 mL/day per animal, administered for 24 hr, and maintained for 7 days.

**Table 1. Experimental groups**

| Groups | Excision wound site | Wound size | Chimney fixation method |
|---|---|---|---|
| TA | Left back (caudal part) | Skin-10 mm diameter, full-thickness (about 1 mm depth)<br>Muscle-8 mm diameter, about 1–2 mm depth | TA only |
| TA + SI (two sites) | | | TA and SI suture (two sites) |
| TA + SI (four sites) | | | TA and SI suture (four sites) |
| PS | | | PS suture only |

TA, tissue adhesive; SI, simple interrupted; PS, purse-string.

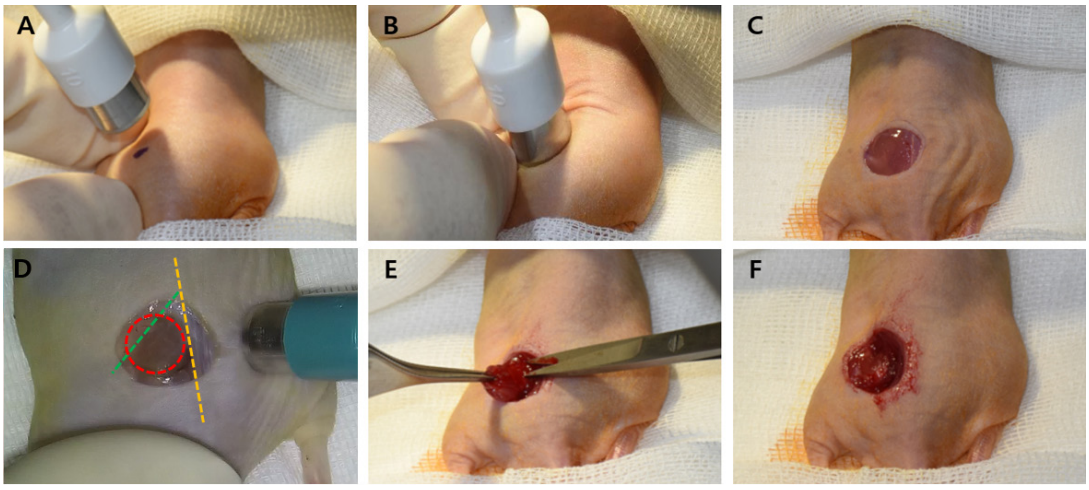


**Fig. 4. Surgical procedure for skin and muscle defect formation.** (A) Landmark of the extensive soft tissue defect (purple dot: greater trochanter of the femur). (B) Formation of the skin defect using a 10-mm biopsy punch. (C) Appearance of the skin defect (10-mm diameter, full-thickness). (D) Formation of the muscle defect using an 8-mm biopsy punch (red circle: defect site; yellow line: spine; green line: gluteal muscle fascia). (E) Formation of the muscle defect using iris scissors. (F) Appearance of the muscle defect (8-mm diameter, 1–2 mm depth).

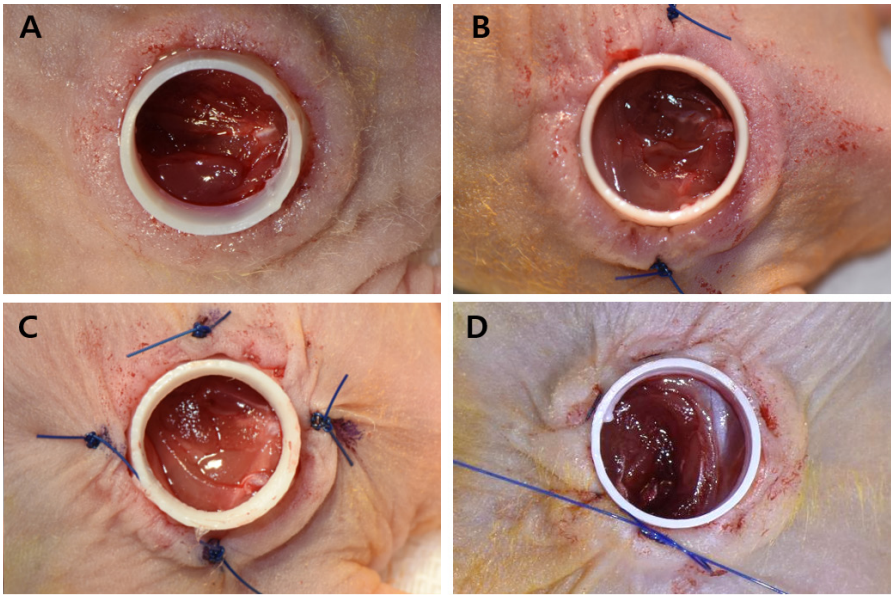


**Fig. 5. Photographs of the chimney application.** (A) Chimney fixation with tissue adhesive only. (B) Chimney fixation with a simple interrupted suture at two sites. (C) Chimney fixation with a simple interrupted suture at four sites. (D) Chimney fixation with a purse-string suture, without tissue adhesive.

The surgical site was inspected daily, and the dressing was reapplied as needed.

### *Sampling*

Euthanasia was performed following the National Institutes of Health guidelines for rodents, using carbon dioxide ($CO_2$). Mice were placed in a 10 L $CO_2$ chamber, and the gas flow rate was gradually increased from 3 L/min to 7 L/min until the mouse lost consciousness. One minute after breathing ceased, the mice were removed from the chamber, and the absence of a heartbeat was confirmed. Hind limb skin and muscle wounds were assessed, and wound tissues (skin and muscle), along with adjacent normal tissues, were collected and fixed in 10%


https://doi.org/10.12729/jbtr.2025.26.4.159

neutral buffered formalin.

### *Histological analysis*

Tissues collected post-euthanasia were prepared for histological analysis. After fixation in 10% neutral buffered formalin for 24 hr, samples were dehydrated through a graded ethanol series and embedded in paraffin. Sections were cut at 4 μm thickness, then heated on a slide warmer at 70°C for 30 min, followed by deparaffinization and dehydration using xylene and a graded ethanol series. The samples were then rinsed with double-distilled water and stained with hematoxylin and eosin (H&E) and Masson's trichrome (MT). After staining and slide preparation, each section was analyzed using the Pannoramic 250 Flash III (3DHISTECH, Budapest, Hungary) to evaluate inflammatory response, cell infiltration, re-epithelialization, and collagen deposition.

## RESULTS

### *In vitro* polylactic acid evaluation

#### *Cytotoxicity test*

Negative control extracts resulted in a mean cell viability of 99.02 ± 3.7%, whereas positive control extracts showed clear dose-dependent cytotoxicity (≤ 70%), confirming assay validity. All PLA chimney extract groups maintained cell viabilities above 85% across all concentrations, indicating no cytotoxicity (Figs. 6 and 7). These findings confirm that the PLA material used for chimney fabrication is highly biocompatible and noncytotoxic under ISO 10993-5 conditions.

### *In vivo* study in mice

#### *Gross examination*

Gross examination revealed that the TA and TA + SI groups exhibited generally severe inflammatory reactions within the wound area and at the chimney fixation site during the first 1–2 weeks after implantation. In some animals, skin tissue necrosis developed at the fixation

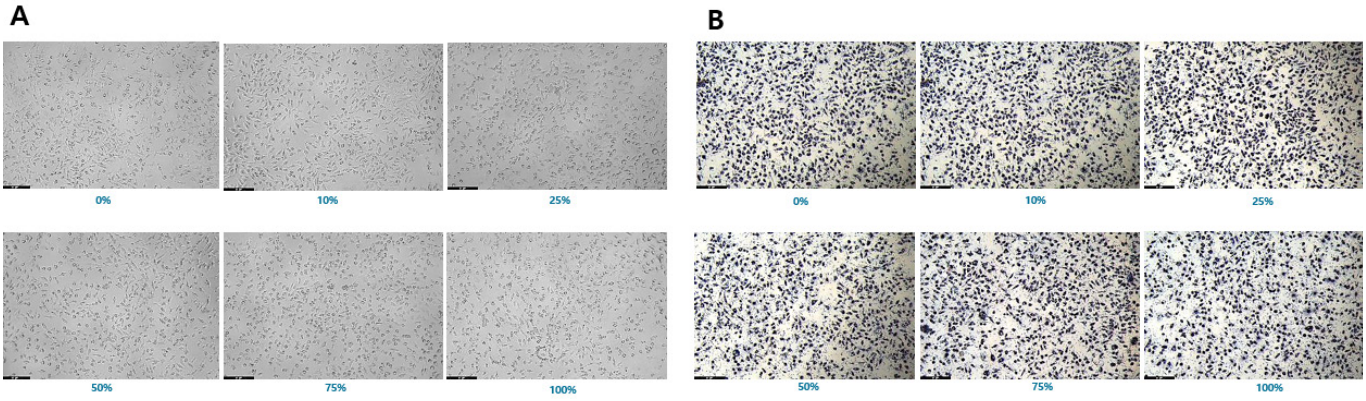


**Fig. 6. Representative morphology of L-929 cells during the cytotoxicity test of PLA materials (× 100).** (A) Cells after exposure to material extracts. (B) Cells after MTT treatment. Scale bars: 100 ㎛. PLA, polylactic acid.

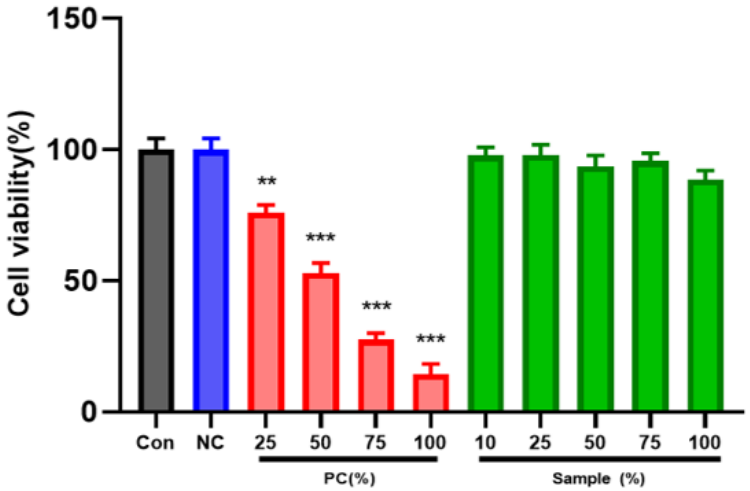


**Fig. 7. Cell viability of L-929 fibroblasts in the MTT cytotoxicity test.** All PLA chimneys maintained cell viability above 85% at all extract concentrations, indicating no cytotoxic effects. Data are expressed as the mean ± S.E. (n = 5). Statistical analysis was conducted using one-way ANOVA. ** $p<0.01$, *** $p<0.001$ vs. control. Con, control; NC, negative control; PC, positive control; PLA, polylactic acid; ANOVA, analysis of variance.

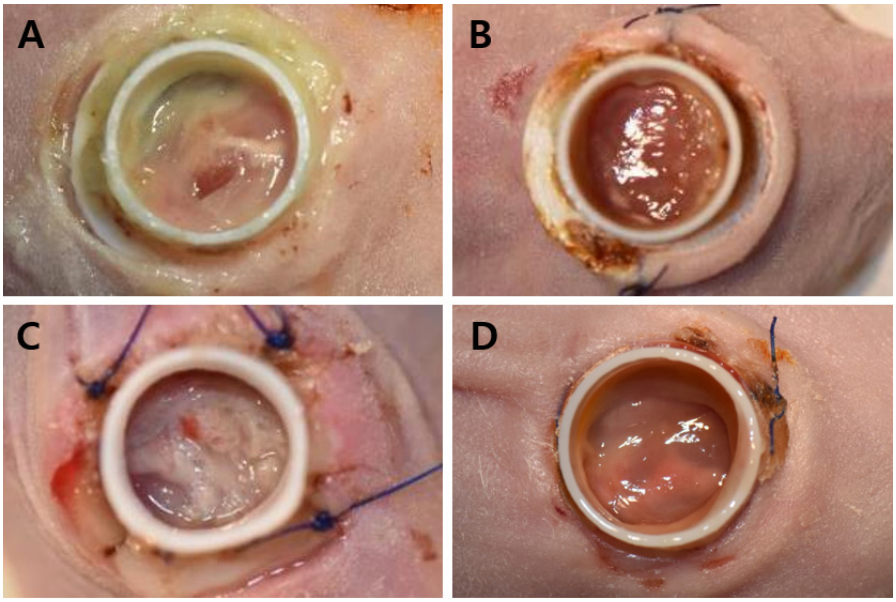


**Fig. 8. Photographs of the wound after chimney fixation with suture techniques and tissue adhesive.** (A) Appearance of the chimney with tissue adhesive 1 week after application. (B) Appearance of the chimney with a two-site simple interrupted suture and tissue adhesive 1 week after application. (C) Appearance of the chimney with four-site simple interrupted suture and tissue adhesive 1 week after application. (D) Appearance of the chimney with purse-string suture 1 week after application.

margins, and the four-suture SI group showed more pronounced inflammation and tissue damage than those of the two-suture SI group (Fig. 8). In contrast, the PS group demonstrated stable chimney retention without inflammation, tissue necrosis, or detachment throughout the 4-week observation period (Fig. 9). These findings indicate that PS fixation offers superior mechanical stability and reduces tissue irritation compared with that of adhesive-based or interrupted-suture fixation.


https://doi.org/10.12729/jbtr.2025.26.4.159

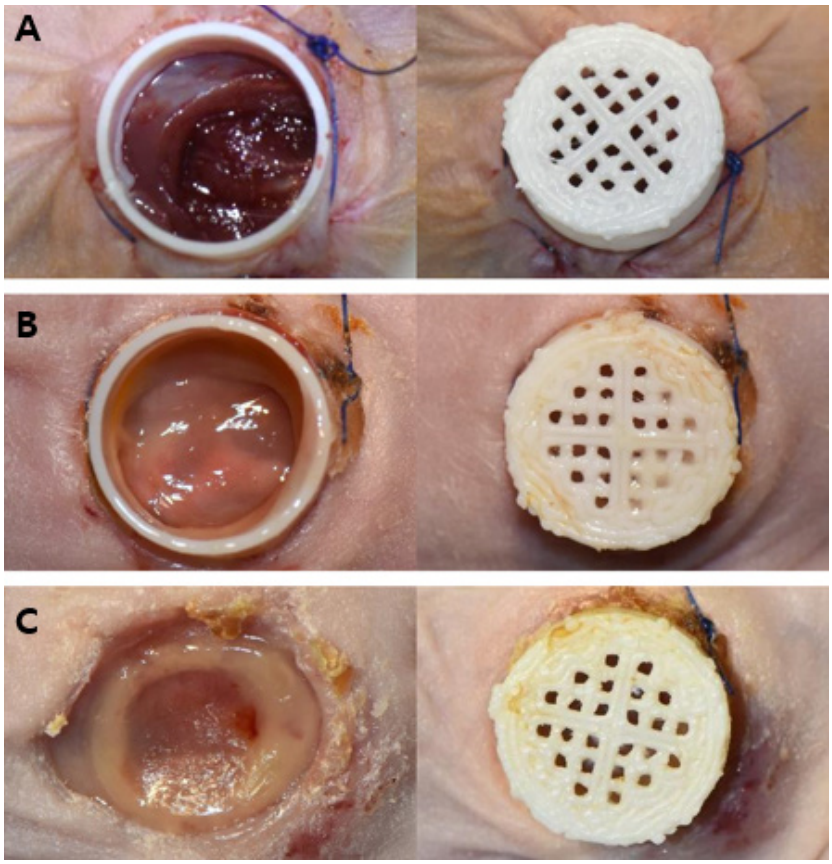


**Fig. 9. Photographs of the wound after chimney fixation with a purse-string suture.** (A) Appearance of the wound, chimney, and lid immediately after application. (B) Appearance of the wound, chimney, and lid 2 weeks after application. (C) Appearance of the wound, chimney, and lid 4 weeks after application.

### *Histopathological assessment*

Histopathological analysis clearly delineated the skin and muscle defect boundaries across all groups. In the TA and TA + SI groups, H&E staining revealed marked inflammatory cell infiltration into the dermis, accompanied by tissue disruption and incomplete wound stabilization (Fig. 10). Conversely, the PS group displayed a well-organized tissue structure with significantly reduced inflammation, consistent with gross findings. MT staining demonstrated distinct structural differences among groups. In the TA and TA + SI groups, extensive collagen deposition and fibrotic tissue accumulation were observed, indicating an exaggerated wound response and instability at the fixation site. In the PS group, collagen fibers were more uniformly aligned, and granulation tissue was firmly established, suggesting effective suppression of contraction and progression toward organized healing.

At higher magnification (Fig. 11), H&E staining revealed active angiogenesis with newly formed, thin-walled blood vessels (Fig. 11A) and dense neutrophil infiltration (Fig. 11B) in the early wound bed. MT staining revealed dense collagen fiber networks and fibrotic connective tissue formation (Fig. 11C), along with abundant spindle-shaped fibroblastic cells (Fig. 11D) occupying the muscle defect region, indicating fibrosis-dominant repair rather than muscle regeneration.

Collectively, these histological findings show that PS fixation combined with the 3D-printed

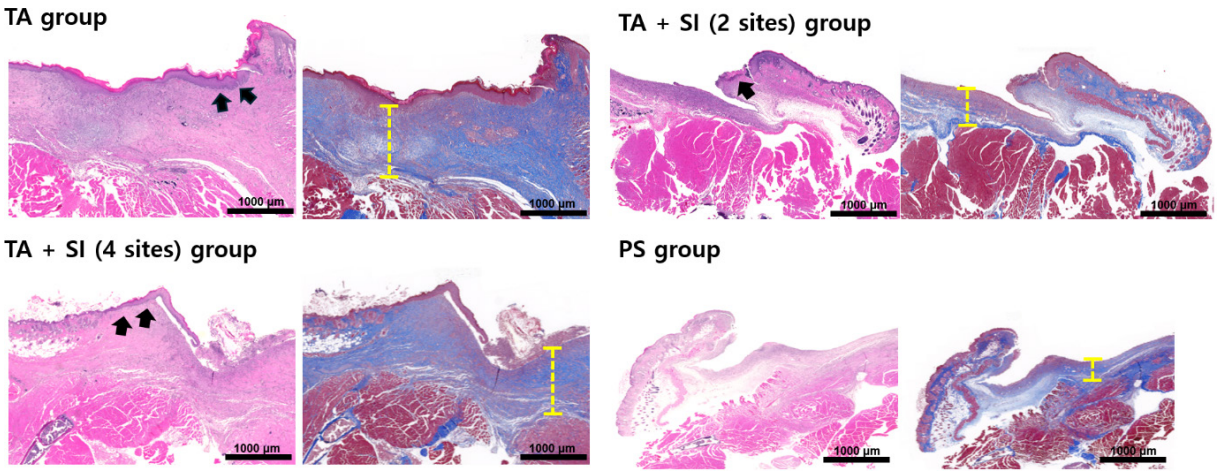


**Fig. 10. Histopathological characteristics of the wound site (H&E and MT staining, low magnification).** H&E staining demonstrates inflammatory cell infiltration into the dermal layer and disrupted wound architecture in the TA and TA + SI groups (black arrows), whereas the PS group exhibits reduced inflammation and more organized wound margins. MT staining shows granulation tissue formation and collagen fiber deposition, with pronounced fibrosis and dense collagen accumulation in the TA and TA + SI groups (yellow line), and more uniform collagen alignment in the PS group, indicating effective suppression of wound contraction. Scale bars: 1,000 ㎛. TA, tissue adhesive; SI, simple interrupted; PS, purse-string; H&E, hematoxylin and eosin; MT, Masson's trichrome.

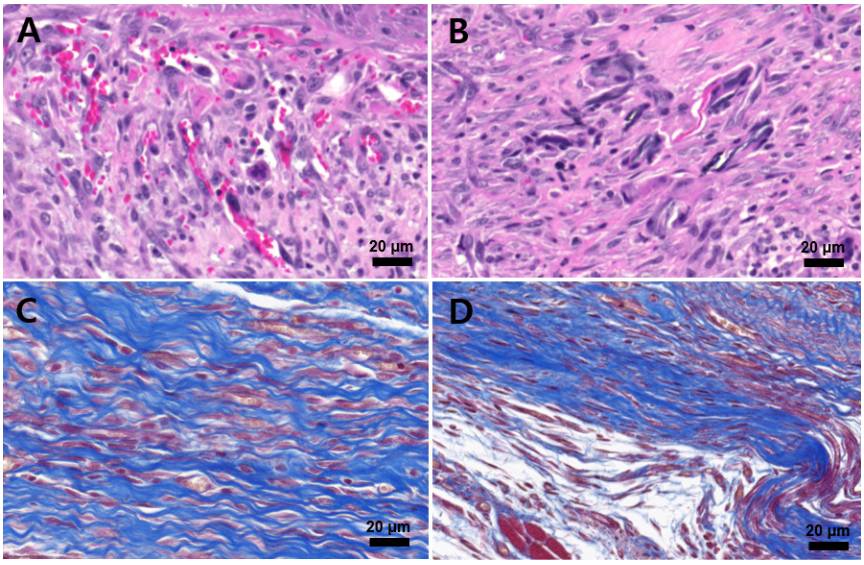


**Fig. 11. Histopathological features of the wound site (H&E and MT staining, high magnification).** (A) H&E staining shows prominent angiogenesis, associated with newly formed capillary-like structures and erythrocyte-filled lumens within the granulation tissue. (B) H&E staining shows dense neutrophil infiltration, indicating an active inflammatory response in the wound bed. (C) MT staining reveals abundant collagen fiber deposition, illustrating progressive extracellular matrix formation and fibrotic remodeling within the defect area. (D) MT staining shows numerous spindle-shaped fibroblast-like cells, consistent with fibrotic connective tissue formation rather than muscle regeneration. Scale bars: 20 ㎛. H&E, hematoxylin and eosin; MT, Masson's trichrome.

chimney suppresses wound contraction, promotes re-epithelialization, and supports organized granulation tissue formation, while adhesive- or suture-based fixation results in excessive inflammation, fibrosis, and structural instability.

## DISCUSSION

In rodents, wounds heal primarily through contraction [10]. In this study, we developed a wound model that better mimics human healing by promoting skin re-epithelialization while


https://doi.org/10.12729/jbtr.2025.26.4.159

simultaneously creating a muscle wound. To prevent contracture, we designed a 3D-printed chimney device for insertion into the wound, replacing conventional silicone or metal splints [14]. The shape of the chimney was adjusted to fit the wound size in nude mice. The initial model had a chimney thickness, wing diameter, and chimney height of 2.6, 10, and 10 mm, respectively. However, when applied to the mice, the thickness and height were excessive, while the wing diameter was inadequate. Consequently, the thickness and height were reduced, and the wing diameter increased to establish the final dimensions of the chimney. The design was then modified according to the fixation method between the chimney and the wound. A chimney without wing holes was initially secured to the surrounding tissue using adhesive. However, after approximately 2 weeks, the adhesive weakened, causing the chimney to detach. To address this, two or four holes were added to the chimney wing, SI sutures were placed at each hole, and the device was further secured with adhesive. As the number of sutures increased, the inflammatory response intensified. In specimens with four sutured sites, the caudal skin surrounding the sutures became necrotic, leading to chimney detachment. This likely occurred because this area is most affected by hand-limb movement. To mitigate inflammation, the holes were removed, and the chimney was secured with a PS suture. Covering the chimney with a mesh-topped lid also helped prevent infection and allowed easier monitoring of the wound during the experiment.

Histopathology confirmed the absence of the panniculus carnosus muscle layer (responsible for contraction) at the wound margin. Re-epithelialization was also observed, indicating that healing progresses in a manner similar to human wound repair. Additionally, granulation tissue was evident in the wound, and repair through fibrous tissue regeneration—including connective and muscle tissue—was confirmed through fibroblasts and collagen deposition. A host-derived neomatrix formed along the defect margin; however, it progressed toward fibrosis rather than muscle regeneration, as typically observed in the VML model [7].

However, this study has some limitations, including a small animal sample and a relatively short follow-up period for assessing skeletal muscle healing. While early outcomes were favorable, long-term studies evaluating muscular layer regeneration or fibrosis are needed [8]. For muscle-layer defect research, the VML model is commonly used, and in rodents, defects are typically created in the tibialis anterior or quadriceps femoris muscles [16–18]. In this experiment, the wound was unavoidably created between the back and hind legs to induce skin and muscle defects. Developing a more refined VML model requires further research to determine whether excessive damage causes functional impairment and to quantify muscle defect formation.

## Conclusion

This study established a mouse soft tissue defect model encompassing skin and muscle layers using a 3D-printed, chimney-shaped PLA splint. The model effectively prevented contraction driven by the panniculus carnosus, the primary wound-healing mechanism in rodents. Comparison of fixation methods revealed that TAs or SI sutures induced severe inflammation, tissue necrosis, and chimney detachment, whereas the PS suture was the optimal method,

maintaining the splint for up to 4 weeks without adverse effects. Furthermore, employing a mesh-topped lid prevented infection and facilitated wound observation.

Histological analysis revealed healing similar to human wound healing, with re-epithelialization progressing from the wound margins and granulation tissue formation within the wound area. The excellent biocompatibility of the PLA material was confirmed through *in vitro* cytotoxicity assays.

Although limited by a small animal cohort and short follow-up for muscle regeneration, this study presents a standardized, reproducible animal model for clinically relevant composite soft tissue defect research. This model could provide a valuable foundation for understanding the complex healing mechanisms of extensive soft tissue defects and evaluating the preclinical efficacy of novel tissue engineering technologies and regenerative medicine therapies.

## REFERENCES


1. Nunan R, Harding KG, Martin P. Clinical challenges of chronic wounds: searching for an optimal animal model to recapitulate their complexity. Disease Model Mech 2014;7:1205-1213.
2. Seo J, Park SJ, Choi JJ, Kang SW, Lim JJ, Lee HJ, Kim JS, Yang HM, Kim SJ, Kim EY, Park SP, Moon SH, Chung HM. Examination of endothelial cell-induced epidermal regeneration in a mice-based chimney wound model. Wound Repair Regen 2016;24:686-694.
3. Gurtner GC, Werner S, Barrandon Y, Longaker MT. Wound repair and regeneration. Nature 2018;453:314-321.
4. Jang KS, Park SJ, Choi JJ, Kim HN, Shim KM, Kim MJ, Jang IH, Jin SW, Kang SS, Kim SE, Moon SH. Therapeutic efficacy of artificial skin produced by 3D bioprinting. Materials 2021;14:5177.
5. Wu J, Matthias N, Bhalla S, Darabi R. Evaluation of the therapeutic potential of human iPSCs in a murine model of VML. Mol Ther 2021;29:121-131.
6. Nakayama KH, Quarta M, Paine P, Alcazar C, Karakikes I, Garcia V, Abilez OJ, Calvo NS, Simmons CS, Rando TA, Huang NF. Treatment of volumetric muscle loss in mice using nanofibrillar scaffolds enhances vascular organization and integration. Commun Biol 2019;2:170.
7. Sicari BM, Agrawal V, Siu BF, Medberry CJ, Dearth CL, Turner NJ, Badylak SF. A murine model of volumetric muscle loss and a regenerative medicine approach for tissue replacement. Tissue Eng Part A 2012;18:1941-1948.
8. Hu C, Chiang G, Chan AHP, Alcazar C, Nakayama KH, Quarta M, Rando TA, Huang NF. A mouse model of volumetric muscle loss and therapeutic scaffold implantation. Nature Protoc 2025;20:608-619.
9. Davidson JM. Animal models for wound repair. In: Murad A, Thanvi G (eds.). Archives of dermatological research. Berlin: Springer; 1998. p. S1-S11.
10. Zomer HD, Trentin AG. Skin wound healing in humans and mice: challenges in translational research. J Dermatol Sci 2018;90:3-12.
11. Sundberg JP, Silva KA, McPhee C, King LE Jr. Skin diseases in laboratory mice: approaches to drug target identification and efficacy screening. In: Proetzel G, Wiles MV (eds.). Mouse



https://doi.org/10.12729/jbtr.2025.26.4.159

models for drug discovery. Berlin: Springer; 2006. p. 193-213.
12. Ansell DM, Holden KA, Hardman MJ. Animal models of wound repair: are they cutting it? Exp Dermatol 2012;21:581-585.
13. Galiano RD, Michaels J 5th, Dobryansky M, Levine JP, Gurtner GC. Quantitative and reproducible murine model of excisional wound healing. Wound Repair Regen 2004;12:485-492.
14. Davidson JM, Yu F, Opalenik SR. Splinting strategies to overcome confounding wound contraction in experimental animal models. Advances Wound Care 2013;2:142-148.
15. Miller AW, Anderson AR, Suarez-Arnedo A, Segura T. Wound healing splinting devices for faster access and use. JID Innov 2024;5:100332.
16. Anderson SE, Han WM, Srinivasa V, Mohiuddin M, Ruehle MA, Moon JY, Shin E, Emeterio SCL, Ogle ME, Botchwey EA, Willett NJ, Jang YC. Determination of a critical size threshold for volumetric muscle loss in the mouse quadriceps. Tissue Eng Part C Methods 2019;25:59-70.
17. Baker HB, Passipieri JA, Siriwardane M, Ellenburg MD, Vadhavkar M, Bergman CR, Saul JM, Tomblyn S, Burnett L, Christ GJ. Cell and growth factor-loaded keratin hydrogels for treatment of volumetric muscle loss in a mouse model. Tissue Eng Part A 2017;23:572-584.
18. Narayanan N, Jia Z, Kim KH, Kuang L, Lengemann P, Shafer G, Bernal-Crespo V, Kuang S, Deng M. Biomimetic glycosaminoglycan-based scaffolds improve skeletal muscle regeneration in a Murine volumetric muscle loss model. Bioact Mater 2021;6:1201-1213.